A 0.5-mm^2 Solar Cell-Powered Biofuel Cell-Input Biosensing System With LED Driving for Stand-Alone RF-Less Continuous Glucose Monitoring Contact Lens

Guowei Chen, *Graduate Student Member, IEEE*, Yue Wang, *Graduate Student Member, IEEE*, Tran Minh Quan, Naofumi Matsuyama, Takuya Tsujimura, and Kiichi Niitsu, *Member, IEEE*

***Abstract*—This letter presents the first solar cell (SC)-powered biofuel cell (BFC)-input biosensing system with pulse interval modulation (PIM) and pulse density modulation (PDM) LED driving capability for continuous glucose monitoring (CGM) contact lenses featuring stand-alone RF-less operation. Power supply from on-lens SCs can eliminate the necessity of wireless power delivery, and LED implementation can eliminate the necessity of wireless communication. By employing the BFC-input approach instead of using a power-hungry potentiostat, powering and sensing components are separated, which reduces the power budget from SCs. The measured power of 28/144 nW at the PIM/PDM mode with a 0.31/0.39-V supply voltage can be managed by the on-lens SCs, enabling a fully stand-alone on-lens operation under office-room ambient light whose typical illumination intensity is 800–1600 lx.**

***Index Terms*—Biofuel cell (BFC) input, glucose monitoring, LED driving, smart contact lens, solar cell.**

I. Introduction

Continuous glucose monitoring (CGM) is essential for diabetes patients to keep glucose balanced and track hypoglycemia/hyperglycemia episodes, which is an unhealthy condition of low/high blood glucose level. Therefore, many products have been designed to ensure low-cost and painless CGM. For example, the implantable sensors under the skin monitor the glucose in the interstitial tissue. However, the commercial products in the market have a battery lifespan of from two weeks to three months. Although a fully passive RFID-based CGM sensor tag has been proposed [1], the large size of several mm^2 resulting from the antenna makes humans physically and mentally resistant to the implantable sensors.

CGM systems integrated on contact lenses [2]–[4] to monitor tear glucose levels are preferable, owing to low invasiveness and relatively large space for an inductive link.

Manuscript received December 2, 2021; revised January 26, 2022; accepted February 10, 2022. Date of publication February 16, 2022; date of current version March 3, 2022. This work was supported in part by the Japan Science and Technology Agency/Precursory Research for Embryonic Science and Technology under Grant JPMJPR2034; in part by the New Energy and Industrial Technology Development Organization Uncharted Territory Challenge 2050; in part by Japan Society for the Promotion of Science; in part by the Council for Science, Technology and Innovation/Cross-ministerial Strategic Innovation Promotion Program (SIP), "Energy systems of an IoE society" Japan Science and Technology Agency (JST); in part by the Grant-in-Aid for Young Scientists (A) from the Ministry of Education, Culture, Sports, Science and Technology under Grant 16H06088; and in part by Ministry of Internal Affairs and Communications/Strategic Information and Communications R&D Promotion Programme (MIC/SCOPE) under Grant 185106001. This article was approved by Associate Editor Qinwen Fan. *(Corresponding author: Kiichi Niitsu.)*

Guowei Chen, Yue Wang, Tran Minh Quan, Naofumi Matsuyama, and Takuya Tsujimura are with the Department of Electronics, Nagoya University, Nagoya 464-8603, Japan.

Kiichi Niitsu is with the Department of Electronics, Nagoya University, Nagoya 464-8603, Japan, and also with PRESTO, JST, Saitama 332-0012, Japan (e-mail: niitsu@nuee.nagoya-u.ac.jp).

Digital Object Identifier 10.1109/LSSC.2022.3151904

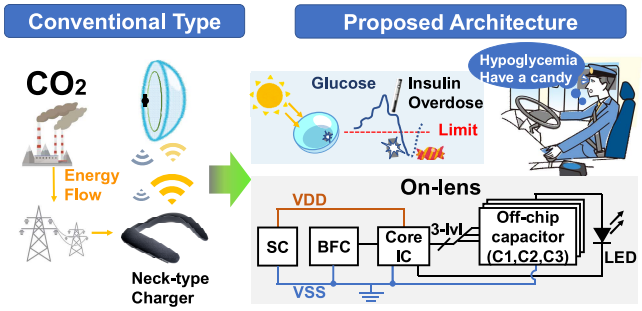

Fig. 1. Conceptual image of the proposed CGM system and its applications.

However, sensing glucose in tears has one major drawback that the correlation between tears and blood varies significantly from person to person, thus lacking accuracy. Therefore, our target application is not to replace the current blood glucose monitor but to provide an auxiliary method for emergency and casual scenarios. Some RFID-based prior studies [2], [4] employed wireless RF power transfer to operate the systems on a contact lens. However, an external device, such as a neck-type charger shown in Fig. 1 transmitting power at a distance of 15 cm [2], is required, which degrades the comfort and health of the users. In addition, wireless power transfer is lossy, incurring low energy efficiency.

Localized energy generation is an effective approach for eliminating the necessity of RF power transfer. A prior study [3] introduced a biofuel cell (BFC) as a power source and achieved wireless data transmission at 0.27 nW at 0.165 V, achieving glucose sensing from the BFC output in the meanwhile. Because BFCs can generate a voltage by themselves through the following chemical reactions:

$$\text{Anode: } C_6H_{12}O_6 + 6H_2O \rightarrow 6CO_2 + 24H^+ + 24e^-$$
$$\text{Cathode: } 6O_2 + 24H^+ + 24e^- \rightarrow 12H_2O$$

while 3-electrode electrochemical sensors cannot, the necessity of a power-hungry potentiostat can be eliminated [5]. However, the unbalanced power link budget requires an external high-gain RF receiver, which is hard to be integrated with a compact size.

Localized information display is an effective approach for eliminating the necessity of external devices, which contributes to a stand-alone RF-less operation. As shown in Fig. 1, by introducing LED displays on lenses driven by off-chip capacitors, the glucose information can be displayed directly to the users unconsciously. Therefore, the users can react to the dramatic glucose level change even during driving a car. However, even dutycycled energy-efficient LEDs require more power than wireless transmitters. Consequently, BFC is only utilized

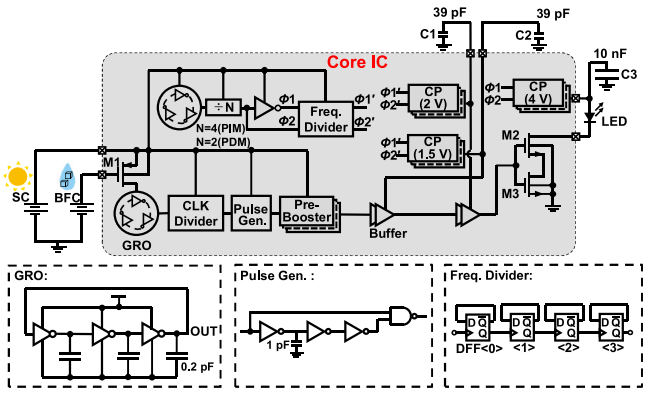

Fig. 2. Block diagram of the proposed SC-powered BFC-input CGM system.

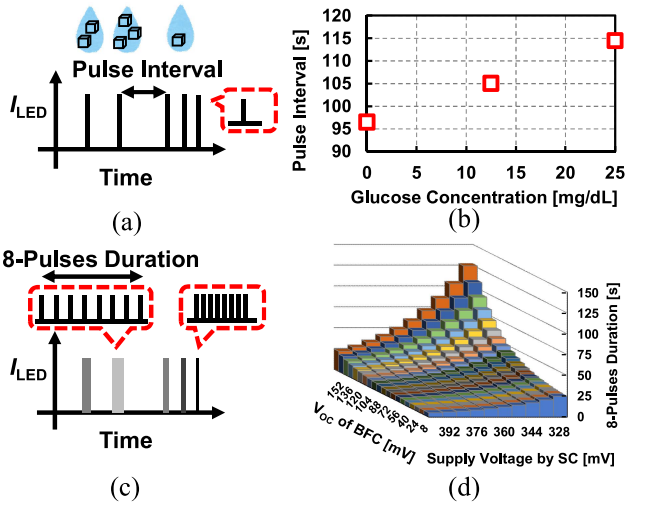

Fig. 3. (a) LED light emission pulse in PIM mode, (b) simulated light emission pulse interval versus glucose concentration, (c) LED light emission pulse in PDM mode, and (d) simulated light emission 8-pulses duration versus V_{OC} of BFC and supply voltage by SC.

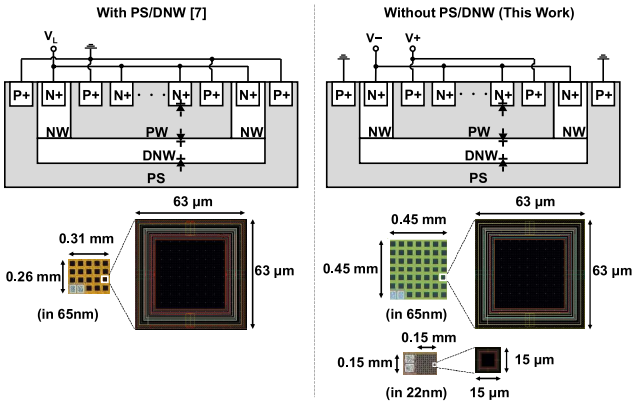

Fig. 4. Cross-section conceptual diagrams, chip micrographs, and layouts of SCs using CMOS process with DNW.

as a sensing element due to its available sub-nW power [6]. The solar cell (SC) is a promising substitute for BFCs as a localized energy harvester for LED driving on contact lenses which can provide 100-s times larger power than BFCs in a unit area [7], but the unstable solar power supply is an obstacle.

Extended from [8], this letter presents the first CGM contact lens by both localized energy generation and information display, with additional details on SC implementations, circuit diagrams, and function validation of the energy harvester across varying light conditions.

II. SC-Powered BFC-Input Biosensing System With LED Driving Capability

Fig. 2 shows the block diagram of the proposed system, including signal modulation, LED driving, and LED switching.

A. Signal Modulation

The nonpotentiostat BFC-input approach separates the sensing component from powering circuits, which reduces the power budget of SCs. Customized 0.6 mm $\times$ 0.6 mm BFC which exhibits an open-circuit voltage (V_{OC}) of 228 mV is developed with a CMOS-compatible process [6]. This kind of BFC has a varying V_{OC} which is proportional to the glucose concentrations. The single pMOS transistor M1 works as a sensing transducer to convert the BFC output voltage into the operating frequency of the gated ring oscillator (GRO). The GRO output is dutycycled by a clock (CLK) divider to output pulses at an interval of several minutes. A pulse generator shortens the width of each pulse to 4 μs for LED blinking light emission, which is distinguishable by the naked human eye [9].

In Fig. 3(a) and (b), an interval-modulated single pulse at the pulse interval modulation (PIM) mode to light the LED is generated with a frequency corresponding to the glucose level. However, the frequency of the GRO is prone to unstable solar power when the users are moving between outdoor and indoor. Therefore, we proposed a pulse density modulation (PDM) mode as shown in Fig. 3(c) to generate seven more pulses in a row as opposed to a single pulse with PIM at the cost of a higher power, so the users can distinguish the glucose level by the density of the LED lighting pulses. Fig. 3(d) shows the 8-pulse duration corresponding to the V_{OC} of BFC and supply voltage by SC, which is confirmed by the post-layout simulation using the SPECTRE simulator. When the BFC output is low, which means a low glucose level, the duration is short and pulse density is high, the frequent LED lighting gives an alert of hypoglycemia. It is worth mentioning that since both SC and BFC can affect the current through the GRO, the system requires a stable light environment such as a bright office room to offer a relatively stable SC output.

B. LED Driving

Fig. 4 shows the details of the SC implementation. Three types of PN junctions, i.e., P-well (PW)/N+, PW/deep-N-well (DNW), and P substrate (PS)/DNW, can be used as photodiodes in the standard triple-well CMOS process. As a counterpart of solar cells [7], this work changes the wire connection to attain a higher open-circuit voltage. In order to provide more power from the constrained area, this work implemented two patterns of SCs with different processes and pitch. The SC in 22-nm CMOS with a smaller pitch can improve the fill factor, thus offering a higher power density.

To drive an LED, charge pumps and a 10-nF off-chip energy storage capacitor (C3) are employed. Although the off-chip

capacitor may make users' eyes uncomfortable, it is required for the energy storage for consecutive LED blinking. Even though off-chip components are implemented, the form factor is acceptable due to its thickness of as thin as 0.3 mm for medical-purpose lenses as well as the existing lenses for intraocular pressure monitoring (Triggerfish). To maintain cost effectiveness, a commonly available off-the-shelf yet relatively large white LED (SCMP13WBC8W1) is employed, whose power consumption is the lowest in its series. The capacitance is determined by considering the light-emitting capability and charge pump drive capability.

A two-phase CLK-driven Dickson charge pump with 18 stages, CP (4 V), upconverts the output voltage to 4 V. The Dickson-topology-based CMOS-switched charge pumps are considered because they can offer a high conversion ratio with moderate efficiency. Besides, it has advantages, such as area efficiency and low complexity, compared with inductor-based charge pumps and bootstrap charge pumps. However, it consumes a large amount of power during the startup process. Therefore, the system is forced to adopt an always-on energy harvester to avoid frequent start and shutdown of the charge pump. After one LED lighting pulse, the charge in capacitors is dissipated, then recharged. According to the post-layout simulation, although there is a voltage drop of 86 mV on CP (4 V) output, the minimum operating current of the LED can be kept above 1.4 mA, higher than the visibility limit which requires 0.5 mA. It is a challenge for consequent eight lighting pulses if the charge dissipates too fast. Therefore, in the PDM mode, the CLK frequency of the main charge pump is doubled. So that the voltage can recover faster and gets ready for the next lighting. However, a higher CLK frequency leads to higher power consumption. It is a tradeoff between PIM and PDM modes.

C. LED Switching

The Dickson charge pump schematic was applied to the CP (2 V) and the CP (1.5 V), which have 26 and 6 stages, respectively. The two charge pumps supply the respective voltage of the two-stage inverter-based buffers with 39-pF off-chip energy storage capacitors (C1 and C2) which are used to drive the gate of stacked nMOS switches (M2 and M3). These two capacitors can be replaced by MIM capacitors with an area overhead of 0.045 mm^2 or MOM capacitors adopting the upper layers at the top of logic circuits to avoid area overhead. Other designs use level shifters [3], [5], [9] or voltage regulators [2], [4] to downconvert voltage levels from the main voltage source. However, both methods will load the main charge pump CP (4 V), leading to a poor output voltage and insufficient charge storage in the capacitor. Therefore, CP (4 V) only supplies the LED and the capacitor. The task of driving the buffers is allocated to CP (1.5 V) and CP (2 V). A more complete system for future improvement should include maximum power point tracking to make the energy harvester operate at high efficiency.

III. Measurement Results

The core IC was implemented in standard 65-nm CMOS technology. The die micrograph and the CGM system are shown in Fig. 5. The proposed system takes 11.4 mm × 8.9 mm, which is comparable to the state-of-the-art

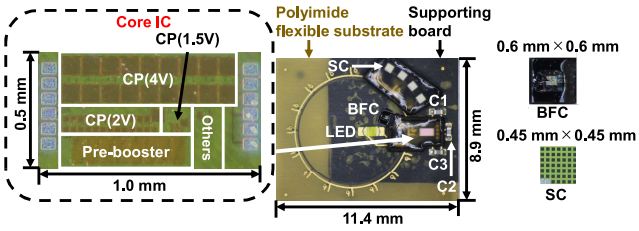

Fig. 5. Chip micrograph of core IC and prototype of the proposed CGM system.

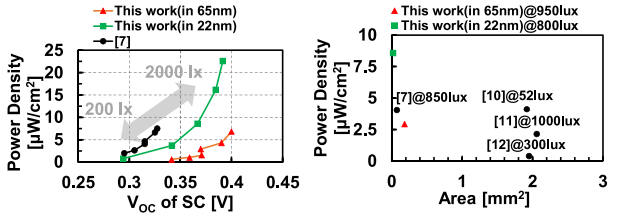

Fig. 6. (a) Measured results of open-circuit voltage and power density of SC units versus light intensity (200–2000 lx). (b) Performance comparison with other on-chip SCs.

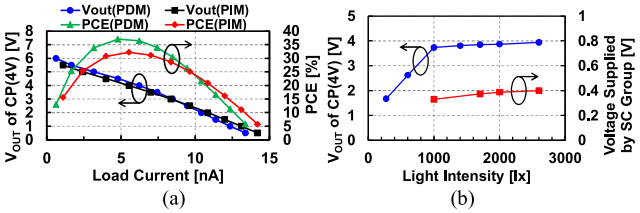

Fig. 7. (a) Performance of CP (4 V) without off-chip C3(10 nF) at 0.39-V supply. (b) Performance of the prototype (in Fig. 6) in different light conditions with four series-connected SCs (in 65 nm).

smart contact lenses [4], [9], whose diameters of the coils are 10 and 11.5 mm, respectively. This system can be integrated on contact lenses with a typical diameter of 14–16 mm. Each component except LED is arranged 3.25-mm away from the eye's central visual axis to avoid vision blocking, since the pupil has a typical diameter of 6 mm.

Fig. 6(a) shows the performance of the SC units. According to the measured I–V characteristics in the illumination intensity range of 200–2000 lx, the SC of this work can supply a higher V_{OC} than the SC in [7]. Fig. 6(b) compares the performance with other on-chip solar cells [10]–[12]. By the same principle of SCs in [10] using a small pitch, the SC of this work in 22 nm achieves the highest power density around 900-lx light intensity because of the high fill factor. By integrating 15 SC chips on the lens, the total available power is sufficient for the operation of the proposed CGM system at 800–1600 lx, which is a typical illumination intensity range in a bright office room.

Fig. 7(a) shows the performance of CP (4 V) without off-chip C3 (10 nF) at 0.39-V supply. The power conversion efficiency (PCE) and output voltage (V_{OUT}) are almost the same in PDM and PIM modes because of the same flying capacitor in the last stage. The higher switching frequency of the PDM mode brings a slight improvement on PCE and V_{OUT} at 4 V, which is the operating point. Although the system is free running without a voltage regulator, the energy harvester works near the maximum power point, because the load

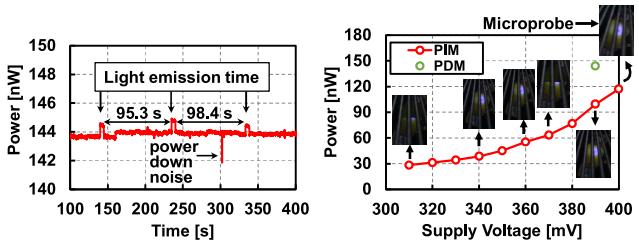

(a) (b)

Fig. 8. (a) Power consumption at 0.39-V supply under PDM mode. (b) Standby power consumption and light emission versus supply voltage.

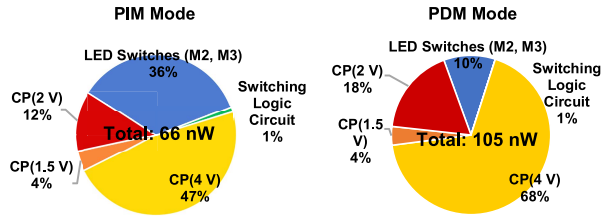

(a) (b)

Fig. 9. Simulated power breakdown in (a) PIM (b) PDM modes.

TABLE I
COMPARISON WITH PREVIOUS WORKS ON CGM CONTACT LENS

	[2] ISSCC'11	[3] BioCAS'18	[4] VLSI'19	This work
Target application	CGM + RFID	CGM + Wireless TX	CGM + RFID	CGM + LED display
Supply voltage [V]	1.2 (regulated)	0.165–0.39	2.0 (regulated)	0.31–0.4 (PIM) 0.39 (PDM)
Energy and sensing source	RF-powered (2.4 GHz)/ Potentiostat	BFC-powered /BFC-input	RF-powered (433 MHz) / Potentiostat	Solar cell-powered /BFC-input
Modulation scheme	FM-LSK	Supply-modulated OOK	LSK + OOK	PIM/PDM
Power	3 µW (only tag)	0.27–11.8 nW (only TX)	143 nW (only tag)	28–117 nW (PIM) 144 nW (PDM)
Off-chip capacitor	None	None	1 (RF mode)	1×10 nF 2×39 pF
External device	RFID Reader/ Writer	Data Receiver	RFID Reader/ Writer	Fully stand-alone
Readout distance	15 cm	> 10 cm	1 cm	Display on lens
Process	0.13 µm	65 nm	0.18 µm	65 nm
Chip area [mm^2]	0.5	0.1482	2.25	0.5
Glucose level [mg/dL]	0–36	180–540	3–25	0–25

is almost capacitive-only. Fig. 7(b) shows the performance of the prototype across varying light conditions. With only four series-connected SCs, the system requires a certain light intensity above 1000 lx to maintain the voltage to drive the LED.

Fig. 8(a) shows the measured power consumption at a 0.39-V power supply under the PDM mode. There were three spikes, which suggest that the LED was lighting at the time. The time intervals between the spikes are 95.3 s when the BFC output is 0 V, which comply with the simulated results in Fig. 3(b). The random power down noise may occur resulting in a delayed time interval to 98.4 s. The light emission time with eight lighting pulses lasted 5 s, which basically agrees with the simulated results in Fig. 3(d). Fig. 8(b) shows the LED light emission and measured standby power consumption as a function of the supply voltage under two modes. Through observation by a digital camera, light emission from LEDs has been successfully confirmed.

Fig. 9 shows the simulated power breakdown in PIM/PDM modes at 0.39-V supply. The charge pumps and the LED driving circuits dominate the power consumption, while the switching logic circuit consumes sub-nW.

Table I depicts the performance comparison. Since our technique does not require additional power of external devices, such as the RFID reader/writer and wireless receivers, it can reduce the total power dramatically.

IV. CONCLUSION

This letter presented the possibility of the emergence of stand-alone RF-less CGM contact lenses which are environment friendly because they do not use lossy wireless power transfer or battery. The SC-powered BFC-input biosensing system showed the feasibility of providing the users with a noninvasive method to prevent hypoglycemia conditions by displaying glucose level information through the on-lens LED. By prototyping IC in 65-nm CMOS, the measured power of 28/144 nW at the PIM/PDM mode with a 0.31/0.39-V supply voltage has been confirmed, enabling a fully stand-alone operation under office-room ambient light.

REFERENCES

[1] Z. Xiao *et al.*, "An implantable RFID sensor tag toward continuous glucose monitoring," *IEEE J. Biomed. Health Inform.*, vol. 19, no. 3, pp. 910–919, May 2015.

[2] Y.-T. Liao, H. Yao, B. Parviz, and B. Otis, "A 3μW wirelessly powered CMOS glucose sensor for an active contact lens," in *Proc. IEEE Int. Solid-State Circuits Conf.*, Feb. 2011, pp. 38–40.

[3] K. Hayashi *et al.*, "A 385μm × 385μm 0.165 V 0.27 nW fully-integrated supply-modulated OOK CMOS TX in 65nm CMOS for glasses-free, self-powered, and fuel-cell-embedded continuous glucose monitoring contact lens," in *Proc. IEEE Biomed. Circuits Syst. Conf.*, Oct. 2018, pp. 1–4.

[4] C. Jeon *et al.*, "A 143nW glucose-monitoring smart contact lens IC with a dual-mode transmitter for wireless-powered backscattering and RF-radiated transmission using a single loop antenna," in *IEEE Symp. VLSI Circuits Dig.*, Jun. 2019, pp. C294–C295.

[5] A. F. Yeknami *et al.*, "A 0.3-V CMOS biofuel-cell-powered wireless glucose/lactate biosensing system," *IEEE J. Solid-State Circuits*, vol. 53, no. 11, pp. 3126–3139, Nov. 2018.

[6] S. Arata, K. Hayashi, Y. Nishio, A. Kobayashi, K. Nakazato, and K. Niitsu, "Wafer-scale development and experimental verification of 0.36mm^2 228mV open-circuit-voltage solid-state CMOS-compatible glucose fuel cell," *Jpn. J. Appl. Phys.*, vol. 57, Mar. 2018, Art. no. 04FM04.

[7] A. Kobayashi *et al.*, "A solar-cell-assisted, 99.66% biofuel cell area reduced, biofuel-cell-powered wireless biosensing system in 65-nm CMOS for continuous glucose monitoring contact lenses," in *Proc. IEEE Int. Conf. Electron. Circuits Syst. (ICECS)*, Nov. 2019, pp. 61–64.

[8] G. Chen *et al.*, "A 0.5 mm^2 0.31 V/0.39 V 28 nW/144 nW 65 nm CMOS solar cell-powered biofuel cell-input biosensing system with PIM/PDM LED driving for stand-alone RF-less continuous glucose monitoring contact lens," in *Proc. IEEE Eur. Solid State Circuits Conf. (ESSCIRC)*, Sep. 2021, pp. 171–174.

[9] J. Pandey, Y.-T. Liao, A. Lingley, R. Mirjalili, B. Parviz, and B. Otis, "A fully integrated RF-powered contact lens with a single element display," *IEEE Trans. Biomed. Circuits Syst.*, vol. 4, no. 6, pp. 454–461, Dec. 2010.

[10] N. Shah, P. Lajevardi, K. Wojciechowski, C. Lang, and B. Murmann, "An energy harvester using image sensor pixels with cold start and over 96% MPPT efficiency," *IEEE Solid-State Circuits Lett.*, vol. 2, no. 9, pp. 207–210, Sep. 2019.

[11] F. Horiguchi, "Integration of series-connected on-chip solar battery in a triple-well CMOS LSI," *IEEE Trans. Electron Devices*, vol. 59, no. 6, pp. 1580–1584, Jun. 2012.

[12] M. Megahed, Y. Ramadass, and T. Anand, "A sub 1μW switched source + capacitor architecture free of top/bottom plate parasitic switching loss achieving peak efficiency of 80.66% at a regulated 1.8V output in 180nm," in *Proc. IEEE Custom Integr. Circuits Conf.*, Apr. 2019, pp. 1–4.